Available online at www.sciencedirect.com
ScienceDirect
Journal of the European Ceramic Society 31 (2011) 2241–2246
www.elsevier.com/locate/jeurceramsoc

Fabrication and laser behaviors of Nd:YAG ceramic microchips

Wang Guo, Yongge Cao*, Qiufeng Huang, Junting Li, Jiquan Huang, Zhi Huang, Fei Tang

Key Laboratory of Optoelectronic Materials Chemistry and Physics, Fujian Institute of Research on the Structure of Matter, Chinese Academy of Sciences, Fuzhou 350002, PR China

Received 11 January 2011; received in revised form 5 May 2011; accepted 16 May 2011
Available online 12 June 2011

Abstract

Transparent Nd:YAG ceramic microchips were fabricated through the slip casting shaping directly from the slurry formed by the commercial $Al_2O_3/Y_2O_3/Nd_2O_3$ powders, and followed by the vacuum sintering procedure. Viscosity of the slurries, the phase evolution and the densification behavior were investigated. For the $Al_2O_3/Y_2O_3/Nd_2O_3$ compound slurries system, the optimal condition is 0.5 wt.% NH_4PAA dispersant and 30 wt.% solid loading at pH $\geq$ 8. The YAG phase started to form at 1250° C and pure YAG phase could be obtained at 1400° C. The optical in-line transmittance of the Nd:YAG ceramics with thickness of 2 mm was about 83.8% at 1064 nm and 82.5% at 400 nm, which hit the upper limit of the theoretically calculated value. For the 1.0 at.% Nd:YAG ceramic microchip, the slope efficiency was 43% for 1.0 at.% Nd:YAG ceramic pumped by 920 mW cw Ti:sapphire tunable laser, and the maximum laser output power 246 W was obtained for 2.0 at.% Nd:YAG ceramics pumped by 925 W LD.

Keywords: YAG creamic; A. Slip casting; A. Sintering; C. Optical properties

1. Introduction

Yttrium aluminum garnet ($Y_3Al_5O_{12}$ or YAG) ceramics have grown to be the focused gain media for high power, high energy solid-state lasers[1,2] due to their unique advantages such as large size, high doping concentration, high fracture toughness, and structural composite of 3-dimensional rare-earth distribution which favor the easy thermal management. Different fabrication routes have been followed[3–6] in which both the Konoshima method[7] and the world lab procedure[8] are demonstrated to be the most successful ones. For Konoshima method, in the beginning, high performance nanosized YAG powders are fabricated through co-precipitation, followed by slip-clasting shaping, and finally densified by vacuum sintering. The large size of 115 mm × 115 mm × 22 mm YAG ceramics have been achieved by this method.[6] For the world lab method, Al_2O_3 and Y_2O_3 powders are used to be cold isostatically pressed followed by vacuum sintered.[8] However, there are some disadvantages for both methods. For the former, it is hard to control the co-precipitation procedure to obtain the uniform and dispersive YAG spherical powders; and for the latter, it is difficult to fabricate the large ceramic slab with super optical uniformity. Here, we report a different simple route for the synthesis of transparent Nd:YAG ceramics, which assimilate the advantages of the two methods mentioned above and is also easy to be controlled to produce large ceramic slabs and microchips. Meanwhile, the laser properties of the as-fabricated ceramic microchips are reported.

2. Experimental procedure

2.1. Ceramic fabrication

Submicron (0.1–0.3 μm) α-Al_2O_3 powder (sumitomo corporation, purity >99.99%), micron (2–6 μm) Y_2O_3 powder (Jiangyin Jiahua Advanced Material Resources Co., Ltd., China, purity >99.99%) and micron (1–2 μm) Nd_2O_3 powder (Alfa Aesar, purity >99.995%) were used as starting materials. 0.2 wt.% MgO (Alfa Aesar, purity >99.99%) and 0.5 wt.% TEOS (Alfa Aesar, purity >99%)were used as sintering aids and a water soluble polyelectrolyte (ammonium polyacrylate, NH_4PAA) was chosen as a dispersant to prepare ceramic slurries. The powders were mixed and ball-milled in deionised water for 24 h. The as-obtained dispersive slurry was casted into a gypsum mold

* Corresponding author. Tel.: +86 591 83721039; fax: +86 591 83713291.
E-mail address: caoyongge@fjirsm.ac.cn (Y. Cao).

0955-2219/$ – see front matter © 2011 Elsevier Ltd. All rights reserved.
doi:10.1016/j.jeurceramsoc.2011.05.020

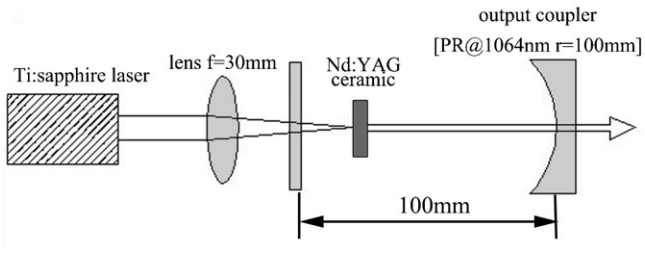

Fig. 1. Schematic of the Ti:sapphire-pumped laser oscillation.

and dried to obtain a desired shape, followed by drying in air at 70 °C and subsequent heating at 700 °C for 2 h. The obtained green compacts were vacuum sintered for different hours under varied temperatures. After annealing and mechanical polishing, the high quality transparent Nd:YAG ceramics were obtained.

Viscosity of the slurries was characterized by rotating viscometer (LVDV-II + PRO, Brookfield, USA). Morphology observation was performed on a JSM-6700F field emission scanning electron microscope (FE-SEM, JEOL, Japan). XRD patterns were recorded using a Rigaku Dmax2500 X-ray diffractometer. The density was measured by the Archimedes method, using deionized water as the immersion medium. The in-line transmittance was obtained by UV/Vis/NIR spectrophotometers (Lambda-900, PerkinElmer, USA).

2.2. Laser experiment

Fig. 1 shows the schematic of the Nd:YAG ceramic laser. The laser cavity is an end-pumped plano-concave resonator. A 1.0 at.% Nd:YAG ceramic microchip (15 mm in diameter and 1 mm in thickness) without any anti-reflection or high-transmission coating was used as the gain medium. A cw 808 nm Ti:sapphire tunable laser (Model 3900 s, Spectra-Physics) with pump-beam radius of about 20 μm was used as the pump source which was focused into the sample through a lens with a 30 mm focal length. The total cavity length was approximately 100 mm, and the sample was held in an aluminum mount and positioned in the middle of the cavity. The input mirror of the laser cavity was 90% transmission at 808 nm and 99.7% reflectivity at 1064 nm. An output coupler with a curvature of 100 mm and 5% transmission was also used.

3. Results and discussion

Fig. 2 shows the SEM micrographs of the starting materials and the green compact obtained by slip casting. The average particle sizes of the Al_2O_3, Y_2O_3 and Nd_2O_3 are about 200 nm, 5 μm and 2 μm, respectively. After processing by ball-milling and slip casting, the as-obtained green compact displays a uniform structure with density of about 33.5% of the theoretical value.

Fig. 3 indicates the viscosity vs. shear rate flow curves for compound slurry as a function of different ammonium polyacrylate concentration from 0.1 wt.% to 1.0 wt.% at pH ≥ 8 and the same solid loadings. It exhibited pseudoplastic flow behavior when the viscosity decreased with increasing shear rate. The rheological properties of the compound slurries were intensively dependent on the content of additive dispersant. When the amount of dispersant increased from 0.1 wt.% to 0.5 wt.%, the viscosity apparently diminished and the characteristic of the slurry was close to Newtonian fluid at 0.5 wt.% concentration dispersant. However, the viscosity began to increase when the content of dispersant was increased to 1.0 wt.% of the solid

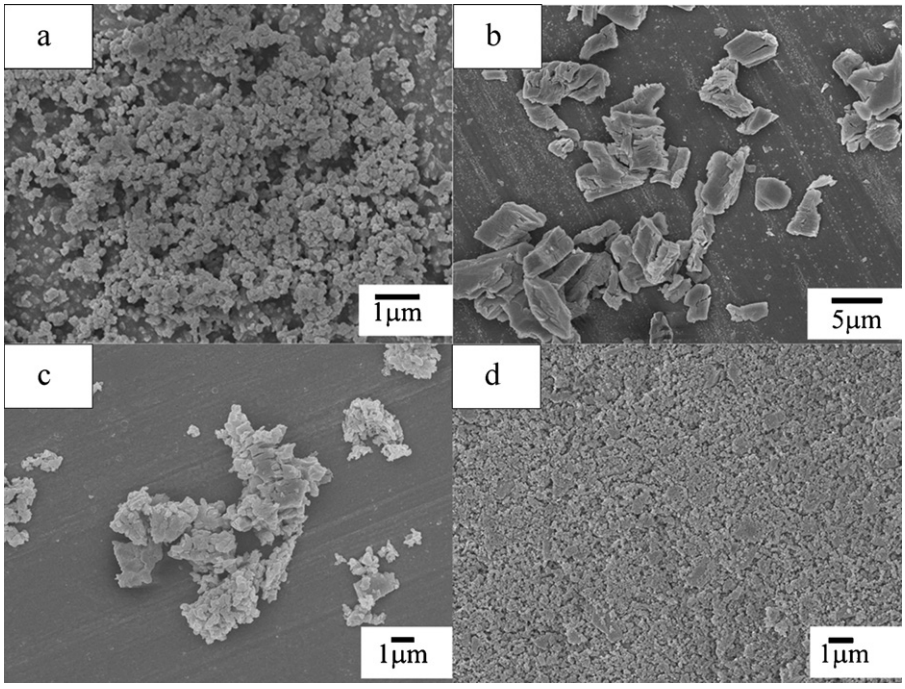

Fig. 2. SEM images of the starting materials: (a) Al_2O_3, (b) Y_2O_3, and (c) Nd_2O_3, and (d) the fracture surface of green compact obtained by slip casting before sintering.

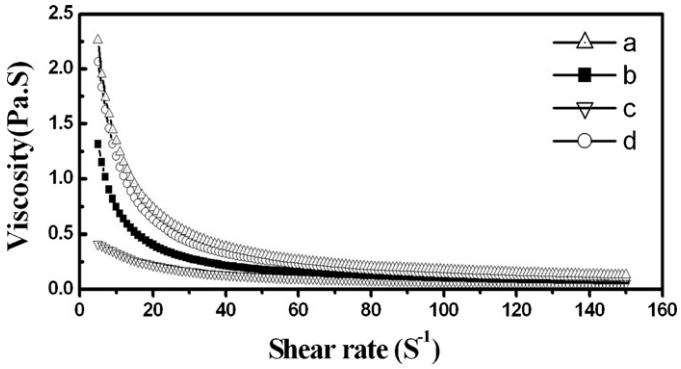

Fig. 3. Viscosity vs. shear rate flow curves for Al_2O_3, Y_2O_3 and Nd_2O_3 compound slurries as a function of different dispersant concentration, (a) 0.1 wt.%, (b) 0.3 wt.%, (c) 0.5 wt.%, (d) 1.0 wt.%.

loading. It signifies that adding dispersant beyond what gives maximum coverage of the surface of the particles would lead to detrimental effects on rheology behavior.

Fig. 4 shows that the rheology behavior of suspensions depends on the solid loadings at pH ≥ 8 and the same amount of dispersant. Near Newtonian fluid was observed at 30 wt.% solid loading, whereas increasing the solid loading obviously enhanced the viscosity of slurries. It showed a shear-thinning behavior with shear rate enlarged. It can be assumed that shearing stress shears off a part of the charge diffuse layer in the solid particle surface. The rheology behavior described by Figs. 3 and 4 can be explained by the following two possible mechanisms[9–11]: firstly, at lower content of deflocculant, the charge density is low and the electrical double layer is thin, so the electrostatic force among particles is not completely screened, which results in the interacted electrostatic attraction in the ceramic particles. As it is well known that higher charge density will cause the increase of electrical double layer thickness, which strengthen the electrostatic repulsive force in each particles. At optimum electrolyte concentration, the zeta potentials of the neighbouring particles set up an ideal equilibrium between attractive and repulsive forces. This leads to optimum repulsion between the particles. Hence the fluid behavior of the slurry is close to ideal Newtonian flow with increasing the amount of dispersant. However, if the amount of dispersant is more than the optimal value, the diffuse layer will become thinner with increasing electrolyte concentration and finally the attractive force will be predominated once again, all of which lead to the tendency of agglomeration and the rheology behavior reduced as shown in Fig. 3. Secondly, the mutual influence of the electrical attraction potentials of neighbour particles must be taken into account, particularly at high solid concentrations. At a low solid concentrations, the distance between particles is so large that the zeta potentials do not overlap. If the solid concentrations is greater, there will be superimposition of the zeta potentials of neighbour raw material particles thus preventing maximum repulsion of neighbour particles, the agglomeration tendency of slips cannot be avoided and lead to augmenting the viscosity of the slurries as shown in Fig. 4. In this system, the optimal condition is 0.5 wt.% ammonium polyacrylate dispersant and 30 wt.% solid loading at pH ≥ 8.

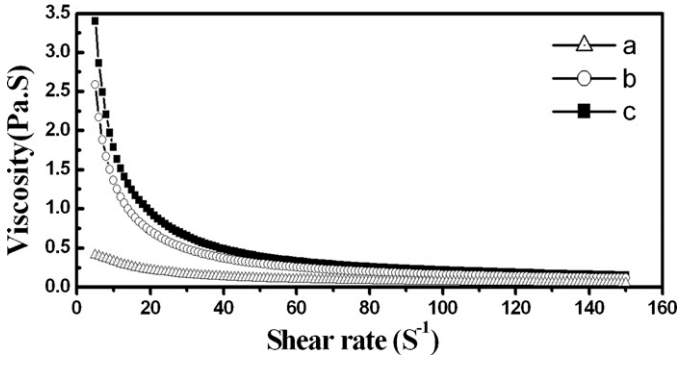

Fig. 4. Viscosity vs. shear rate flow curves for the suspensions prepared at different solid loadings, (a) 30 wt.%, (b) 40 wt.%, (c) 55 wt.%.

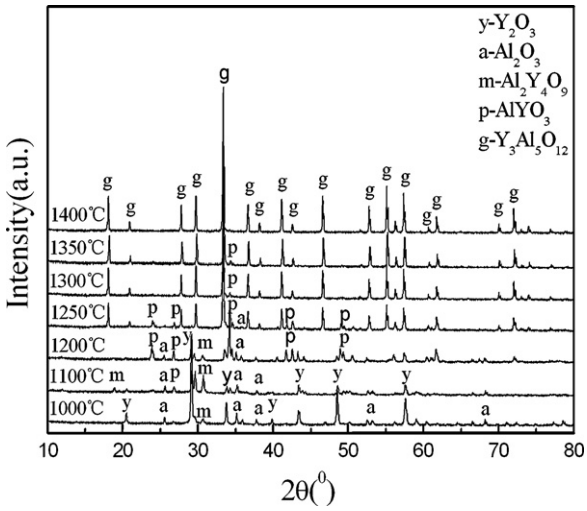

Fig. 5. The XRD patterns of the 1.0 at.% Nd:YAG green compacts calcined for 5 h under different temperatures from 1000 °C to 1400 °C.

Fig. 5 shows the phase transformation of 1.0 at.% Nd:YAG green compacts calcined for 5 h at temperatures from 1000 °C to 1400 °C. In the Al_2O_3–Y_2O_3 system, it is well-known that there are three phases, i.e., monoclinic phase YAM($Y_4Al_2O_9$), perovskite phase YAP($YAlO_3$) and cubic phase YAG($Y_3Al_5O_{12}$). And their formations depend on different sintering temperatures, as shown in Fig. 5. At 1000 °C, the ceramic was mainly composed by Y_2O_3 and Al_2O_3 with minor YAM phase. With increasing the temperature to 1100 °C, the peak intensity of YAM enhanced, which indicated the increase of YAM content. However, the YAM content decreased with further increasing the temperature and finally disappeared at 1250 °C. The YAP phase was first observed at 1100 °C and the YAG phase began to form at 1250 °C. It was found that the higher temperature (>1250 °C) would promote the reaction between YAP and Al_2O_3 and led to the formation of pure YAG phase at temperature of 1400 °C. Based on the XRD observation, the formation of YAG phase can be depicted as follows:

$$2Y_2O_3 + Al_2O_3 \rightarrow Y_4Al_2O_9 \qquad 1000–1100\,^{\circ}C$$

$$Y_4Al_2O_9 + Al_2O_3 \rightarrow 4YAlO_3 \qquad 1100–1250\,^{\circ}C$$

$$3YAlO_3 + Al_2O_3 \rightarrow Y_3Al_5O_{12} \qquad 1250–1400\,^{\circ}C$$

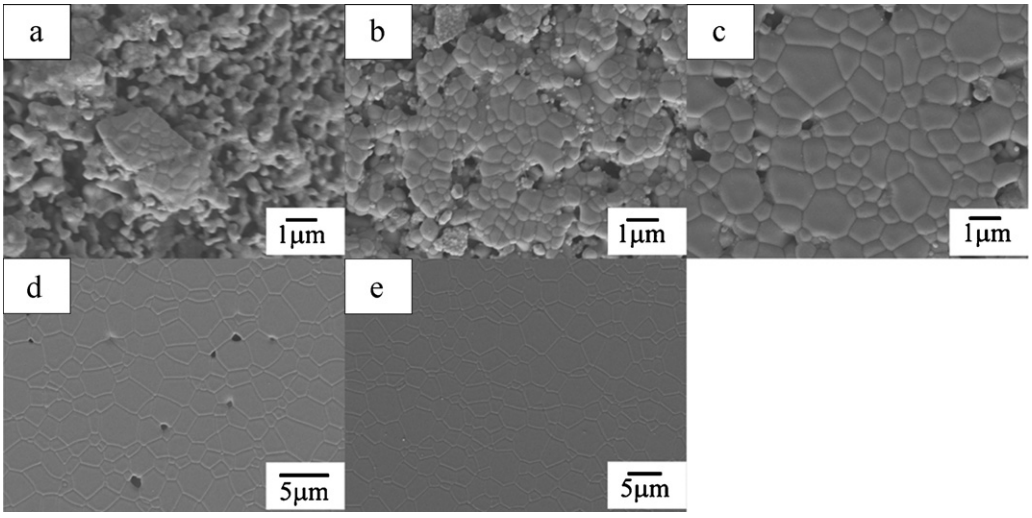

Fig. 6. SEM surface morphologies of the 1.0 at.% Nd:YAG green compacts sintered under vacuum for 5 h at (a) 1400 °C, (b) 1500 °C, (c) 1600 °C, (d) 1700 °C, and (e) 1800 °C, respectively.

Compared with the formation temperatures for YAG phase at 1600 °C by Ikesue[12] and at 1500 °C by Lee,[13] here we report the temperature is much lower. The YAG phase started to form at 1250 °C and pure YAG phase could be obtained at 1400 °C. This may be due to the fact that we used much coarser Y_2O_3 and Nd_2O_3 particles with narrow size distribution as raw materials. In addition, the density of our green compact is lower than that of reported,[12,13] which indicate that the density of the green compact has no effect on the formation temperature of YAG phase. While the grain diameter and distribution of the starting powders should be an important factor for the formation of YAG phase.

The SEM morphologies of the 1.0 at.% Nd:YAG green compacts sintered for 5 h under vacuum are shown in Fig. 6 as a function of the sintering temperatures from 1400 °C to 1800 °C. Fig. 7 shows the dependence of the relative densities and grain sizes sintered at corresponding temperatures. In Fig. 6, it was observed that the sample was loose at 1400 °C and the green compact began to be sintered at 1500 °C. The pores disappeared quickly with further increasing temperatures, and the "pore-free" microstructure was observed at 1800 °C. It was found that both the relative density and the grain size increased with increasing the temperature as shown in Fig. 7. From 1400 °C to 1550 °C, the density increased from 74.6% to 89.5% while the grain size only enlarged from 0.3 μm to 0.7 μm; but from 1700 °C to 1800 °C, the density only increased from 98.7% to 99.9%, while the grain size enlarged from 2.7 μm to 4.5 μm.

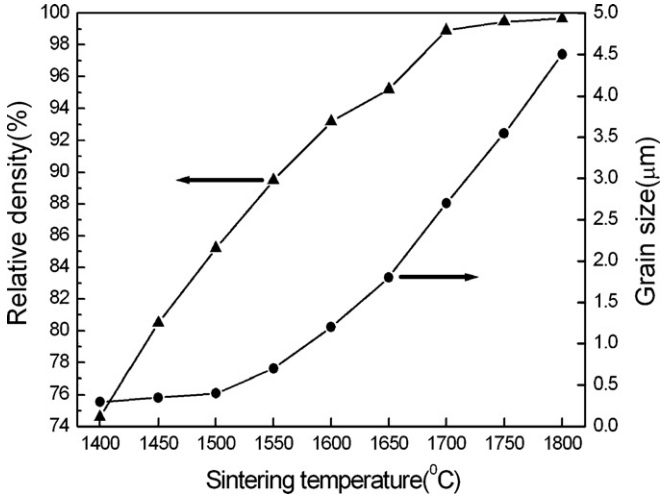

Fig. 7. The relative density and grain sizes vs. temperatures for 1.0 at.% Nd:YAG green compacts sintered under vacuum for 5 h from 1400 °C to 1800 °C.

Obviously, the densification process of the ceramic was mainly performed at lower temperatures (1400–1700 °C), and higher temperatures (1600–1800 °C) mainly promoted the elimination of the residual pores and the rapid grain growth, as indicated in Fig. 6.

Fig. 8 shows the SEM surface morphologies for the polished 1.0 at.% Nd:YAG transparent ceramics sintered at 1800 °C for

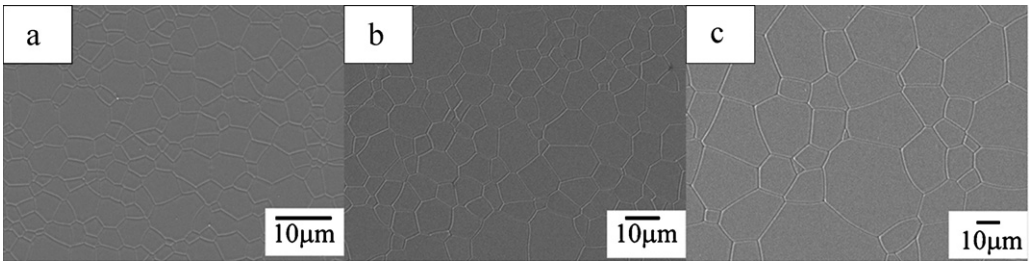

Fig. 8. The SEM surface morphologies for the polished 1.0 at.% Nd:YAG transparent ceramics sintered at 1800 °C under vacuum for (a) 10 h and (b) 20 h with MgO sintering aid, and for (c) 20 h with SiO_2 sintering aid.

10 h and 20 h under vacuum, Fig. 8(a) and (b) are the results with MgO sintering aid and Fig. 8(c) indicates the result with SiO_2 sintering aid. Three samples were pore free and there was no evidence for abnormal grain growth. The average grain sizes for Fig. 8(a) and (b) were about 6 μm and 10 μm, respectively. However, the average grain size was greatly increased to 30 μm for Fig. 8(c) with SiO_2 as sintering aid at the same sintering temperature. It is suggested that high temperature boost the rapid grain growth with increasing duration time. The mean size of 50 μm was also reported by Lee[13] in which the TEOS was used as the sintering aid for the 1.0 at.% Nd:YAG ceramic sintered at 1800 °C for 16 h. It is indicated that the mean grain size for sample with MgO as sintering aid is much smaller than that with SiO_2 as sintering aid. The similar results had been also observed by de with.[14] It is well known that MgO can inhibit the moving of the grain boundary and restrain the growth rate of the grain. Consequently, abnormal growth can be hindered and small grain size can be obtained. Moreover, Mg^{2+} can diffuse into the crystal lattice of YAG and occupy Al^{3+} sites during high-temperature sintering. The replacement of Al^{3+} by Mg^{2+} may accompany the formation of oxygen vacancy as $2MgO \rightarrow 2Mg_{Al}' + V_{\ddot{o}} + O_2$, and thus oxygen vacancies are predominant in YAG, which can accelerate the pores moving out from green compact. The uniform microstructure and extremely low pore volume can significantly reduce the scattering loss in the laser transparent ceramics.

The polished transparent ceramics sintered at 1800 °C are shown in Fig. 9. Although the full transparency can be seen clearly in Fig. 9, the in-line transmittances of both samples were different as shown in Fig. 10. The optical transmittance of sample sintered at 1800 °C for 20 h hit the upper limit of the theoretically calculated values of above 82.5% @ 400 nm and 83.8% @ 1064 nm,[15] while another sample sintered for 10 h at 1800 °C shows a lower transparency.

Fig. 11 shows the 1064 nm laser output power dependence on the absorbed pump powers for the 1.0 at.% Nd:YAG transparent ceramic. The laser threshold was found to be 30 mW. When the pump power reached 86.5 mW, a laser output power of 24.5 mW was obtained. And a laser output power of 385 mW was obtained with a maximum absorbed pump power of 920 mW. The slope efficiency and optic–optic transformation efficiency were 43% and 41.8%, respectively.

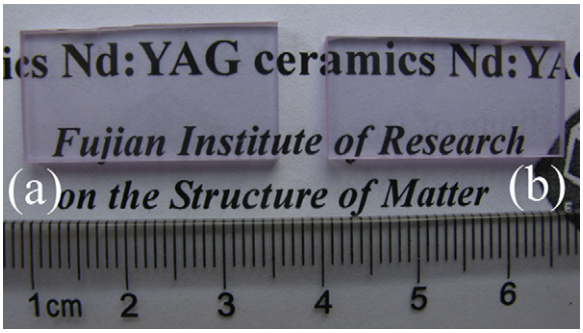

Fig. 9. Photographs of the polished 1.0 at.% Nd:YAG ceramics (2 mm in thickness) sintered at 1800 °C under vacuum for (a) 20 h, and (b) 10 h.

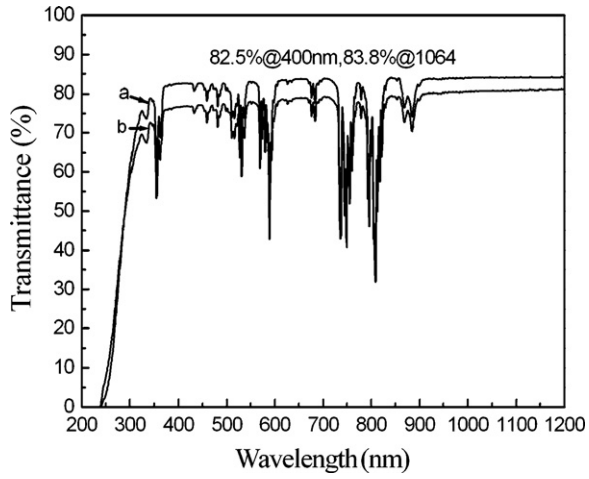

Fig. 10. Optical transmittance of 1.0 at.% Nd:YAG ceramics (2 mm thick) sintered at 1800 °C under vacuum for (a) 20 h and (b) 10 h.

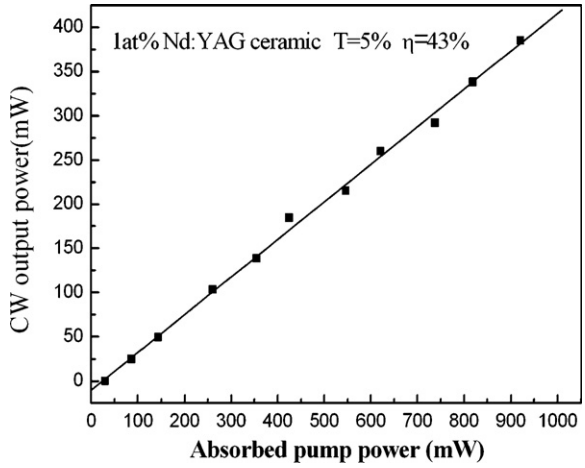

Fig. 11. Laser output power as a function of the absorbed pump power for the 1.0 at.% Nd:YAG transparent ceramic.

For further investigation, the low power Ti:sapphire pump source was changed to a high power LD array of 808 nm. The sample size is around Φ 50 mm × 2.5 mm and the Nd dopent concentration is 2 at.%. The testing parameters for the solid-state laser system are as follows: the cavity length is 0.5 m, the curvature radius of the fully reflecting mirror is 5 m, the transmittance for the output mirror is 8%, the pulse width is 250 μs with repetition frequency of 150 Hz, and the effective pump power is 925 W. Finally, the 246 W laser output at 1064 nm was realized with 32% optical–optical efficiency.

4. Conclusions

Highly transparent polycrystalline Nd:YAG ceramics were fabricated by slip casting shaping, directly from the mixed slurry composed of Al_2O_3, Y_2O_3, Nd_2O_3 powders, followed by vacuum sintering. Viscosity of the slurries, the phase evolution and the densification behavior were investigated. For the $Al_2O_3/Y_2O_3/Nd_2O_3$ compound slurries system, the optimal condition is 0.5 wt.% ammonium polyacrylate dispersant and

30 wt.% solid loading at pH ≥ 8. Pure YAG phase was obtained when the sintering temperature was higher than 1400 °C. The densification process of the ceramic was mainly performed at lower temperatures (1400–1700 °C), and higher temperatures (1600–1800 °C) mainly promoted the elimination of the residual pores and the rapid grain growth. Pore-free 1.0 at.% Nd:YAG transparent ceramics with an average grain size of about 10 μm were obtained when sintered at 1800 °C for 20 h. However, the average grain size is 30 μm with SiO_2 as sintering aid at the same sintering temperature. The in-line transmittances were 83.8% at 1064 nm and 82.5% at 400 nm, which hit the upper limit of the theoretically calculated values. For its laser behavior, When pumped by cw Ti:sapphire tunable laser, the slope efficiency and optic–optic transformation efficiency were 43% and 41.8%, respectively. The maximum output power was 248 W when pumped by 925 W LD. These results show that the as-prepared Nd:YAG ceramic can be used as a highly efficient laser material.

Acknowledgements

This work was supported by the National Natural Science Foundation of China (91022035), and the Key Program of Science and Technology in Fujian Province (2009H0045).

References

1. Ikesue A, Aung YL. Ceramic laser materials. *Nat Photon* 2008;**2**: 721–7.
2. Yagi H, Bisson JF, Ueda K, Yanagitani T. $Y_3Al_5O_{12}$ ceramic absorbers for the suppression of parasitic oscillation in high-power Nd:YAG lasers. *J Lumin* 2006;**121**:88–94.
3. Gong H, Tang DY, Huang H. Agglomeration control of Nd:YAG nanoparticles via freeze drying for transparent Nd:YAG ceramics. *J Am Ceram Soc* 2009;**92**:812–7.
4. Kopylov YL, Kravchenko VB, Bagayev SN, Shemet VV, Komarov AA, Karban OV, et al. Development of Nd:$Y_3Al_5O_{12}$ laser ceramics by high-pressure colloidal slip-casting (HPCSC) method. *Opt Mater* 2009;**31**:707–10.
5. Sato Y, Saikawa J, Taira T, Ikesue A. Characteristics of Nd-doped $Y_3ScAl_4O_{12}$ ceramic laser. *Opt Mater* 2007;**29**:1277–82.
6. Yagi H, Yanagitani T, Takaichi K, Ueda K, Kaminskii AA. Characterizations and laser performances of highly Nd^{3+}:$Y_3Al_5O_{12}$ transparent laser ceramics. *Opt Mater* 2007;**29**:1258–62.
7. Lu JR, Ueda K, Yagi H, Yanagitani T, Akiyama Y, Kaminskii AA. Neodymium doped yttrium aluminum garnet ($Y_3Al_5O_{12}$) nanocrystalline ceramics – a new generation of solid state laser and optical materials. *J Alloys Compd* 2002;**341**:220–5.
8. Ikesue A, Furusato I, Kamata K. Fabrication of polycrystalline, transparent YAG ceramics by a solid-state reaction method. *J Am Ceram Soc* 1995;**78**:225–8.
9. Appiagyei KA, Messing GL, Dumm JQ. Aqueous slip casting of transparent yttrium aluminum garnet (YAG) ceramics. *Ceram Int* 2008;**34**:1309–13.
10. Li X, Li Q. YAG ceramic processed by slip casting via aqueous slurries. *Ceram Int* 2008;**34**:397–401.
11. Naito M, Fukuda Y, Yoshikawa N, Kamiya H, Tsubaki J. Optimization of suspension characteristics for shaping processes. *J Eur Ceram Soc* 1997;**17**:251–7.
12. Ikesue A, Kinoshita T, Kamata K, Yoshida K. Fabrication and optical properties of high-performance polycrystalline Nd:YAG ceramics for solid-state lasers. *J Am Ceram Soc* 1995;**78**:1033–40.
13. Lee SH, Kochawattana S, Messing GL, Dumm JQ, Quarles G, Castillo V. Solid-state reactive sintering of transparent polycrystalline Nd:YAG ceramics. *J Am Ceram Soc* 2006;**89**:1945–50.
14. de with G, van Dijk HJA. Translucent $Y_3Al_5O_{12}$ ceramics. *Mater Res Bull* 1984;**19**:1669–74.
15. Kochawattana S, Stevenson A, Lee SH, Ramirez M, Gopalan V, Dumm J, et al. Sintering and grain growth in SiO_2 doped Nd:YAG. *J Eur Ceram Soc* 2008;**28**:1527–34.